# Hall measurements on low-mobility thin films

Florian Werner

# Hall measurements on low-mobility thin films

Florian Werner[a)]

*Laboratory for Photovoltaics, University of Luxembourg, Rue du Brill 41, L-4422 Belvaux, Luxembourg*

We review the conventional measuring standard for dc Hall measurements in van der Pauw configuration with particular focus on the challenges arising from a small Hall signal compared to sizable offset voltages, which is a typical scenario for many material systems, particularly low-mobility thin films. We show that the conventional approach of using a simple field-reversal technique is often unsuited to obtain reliable results, and present an improved correction scheme to extend the accessible measurement range to mobility values well below $1 \, \mathrm{cm^2/(V \, s)}$. We discuss procedures to limit the impact of temperature fluctuations and long stabilization times for highly resistive materials. We further address potential sources of error due to the presence of grain boundaries in polycrystalline specimen and due to multi-carrier conduction, both of which might yield low apparent Hall mobilities significantly underestimating the actual mobility. © 2017 Author(s). All article content, except where otherwise noted, is licensed under a Creative Commons Attribution (CC BY) license (*http://creativecommons.org/licenses/by/4.0/*). https://doi.org/10.1063/1.4990470

## I. INTRODUCTION

Measurements of the Hall effect[1] and resistivity form the most important technique to directly obtain the charge carrier concentration and mobility of a conductive specimen. Its wide-spread use as a simple and fast routine measurement technique is certainly also based on the simplicity of the van der Pauw formalism,[2,3] which no longer requires precise micro-structuring during sample preparation.

In many modern material systems and devices, the materials of interest are thin films of polycrystalline or amorphous material. On the one hand, Hall measurements on these films are challenging due to their low mobility and high sample resistance. On the other hand, the lack of crystallinity violates the assumption of lateral homogeneity fundamental to the derivation of the van der Pauw formalism. In this regard, the status of the Hall effect as a well-established and understood technique also entails a certain danger; it appears tempting to follow the standard approach of Hall measurements published in text books, without detailed consideration of possible limits and deficiencies of the technique. Thus, a wealth of experimental data is discarded due to apparent inconsistencies in the measurement, and the sample under investigation is deemed unsuited for Hall analysis.

Different ac Hall effect techniques have been developed[4–8] to overcome these challenges in measuring low-mobility materials, and promise an improved sensitivity to small Hall voltage variations compared to the dc Hall effect. Nevertheless, ac techniques might pose additional difficulties regarding the interpretation, electronics setup, and treatment of parasitic resistances and capacitances. Due to these problems and due to the wide-spread use and availability of dc Hall measurement equipment, the dc Hall effect in van der Pauw configuration remains the prevalent Hall measurement technique in many laboratories.

In this paper, we review the conventional measuring standard for dc Hall measurements in van der Pauw configuration, and show how these procedures can be modified to extend the reliable measurement range to mobility values well below $1 \, \mathrm{cm^2/(V \, s)}$.

In Sec. II, we will first review the basic equations governing the analysis of Hall effect measurements in van der Pauw geometry. Special attention will be given to the correction of undesired voltage offsets, which often lead to a misinterpretation of the measured data. We end this section by addressing the particular challenges encountered in measurements of low-mobility thin films, which are for example commonly applied in thin-film photovoltaics. The misalignment voltage is the most limiting factor in the analysis of typical low-mobility thin films, and Sec. III demonstrates that the conventional correction procedures are often unsuited to obtain a reliable result. We present an improved correction scheme based on the zero-field van der Pauw equations, and compare the different offset correction schemes on experimental data showing a hole mobility well below $1 \, \mathrm{cm^2/(V \, s)}$. In Sec. IV, we address potential errors due to insufficient stabilization times and the impact of even minute temperature variations for highly resistive samples. In particular, we address alternative measurement procedures for samples where voltage transients over several minutes might extend the measurement time required for a full van der Pauw analysis to many hours or even days.

After these considerations on the measurement and correction procedures themselves, Sec. V will address the interpretation of apparently low mobility values obtained from Hall measurements: the presence of grain boundaries in polycrystalline material and current conduction by multiple ensembles of charge carriers might both result in a low apparent mobility, several orders of magnitude lower than the actual mobility.

Throughout this paper we shall consider $Cu(In,Ga)Se_2$ thin-film solar cells (for a review see Refs. 9 and 10) as

a)florian.werner@uni.lu

**122**, 135306-1

practically relevant example. Here, the dopant concentration and mobility in the polycrystalline Cu(In,Ga)Se$_2$ absorber and the transparent conductive oxide (TCO) front contact are examples of crucial—but difficult to obtain reliably—device parameters accessible by Hall measurements. Our discussion, however, applies equally to any other low-mobility material measured in van der Pauw configuration.

## II. BASIC THEORY OF HALL EFFECT MEASUREMENTS IN VAN DER PAUW CONFIGURATION

The Hall effect discovered by Hall in 1879[1] and the basic equations governing the analysis of Hall measurements have been presented in a multitude of papers and text books [see, for example, Refs. 11–13]. Hence, only a short summary of the standard procedure will be given here.

Initially, we shall assume a rectangular sample with constant thickness $d$, where a current $I$ of one type of charge carriers flows parallel to the sides as sketched in Fig. 1(a). If a magnetic field $B$ is applied perpendicular to the sample surface, the charge carriers in motion will be deflected by the Lorentz force. The transversal Lorentz force will be compensated by an electric field building up due to the redistribution of mobile charge carriers. In the steady-state, the transversal current will be zero, and we measure a Hall voltage between the opposite sides of the sample. This Hall voltage is given by

$$V_H = \frac{R_H I B}{d},$$  (1)

where $d$ is the film thickness, and


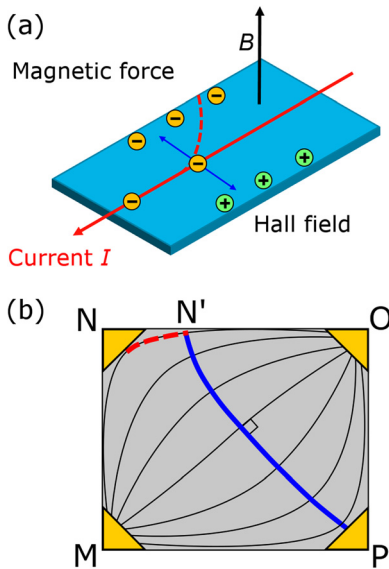
(a) Magnetic force

Current $I$

(b)

FIG. 1. (a) Sketch of the Hall effect in an idealized thin bar-type sample with magnetic field perpendicular to the conductive plane, assuming electron conduction. (b) Sketch of a typical Hall specimen in van der Pauw configuration. Thin lines qualitatively represent current stream lines for current flow between contacts M and O. Contacts N and P are voltage probes. For non-ideal sample geometries, the blue solid line (P-N′) indicates the integrated Hall voltage perpendicular to the current stream lines, while the red dashed line (N′-N) represents the origin of the misalignment voltage.

$$R_H = \pm \frac{r}{qn} = \pm r\rho\mu$$  (2)

is the Hall coefficient, $r$ is the Hall scattering factor, and $R_H > 0$ for holes, $R_H < 0$ for electrons. Accordingly, the majority carrier concentration and mobility can be calculated if the Hall voltage $V_H$ and the sample resistivity $\rho$ are known.

The Hall scattering factor $r$ in Eq. (2) accounts for the energy-dependence of the scattering rate and typically assumes values of around $r \approx \frac{1}{2}$–2, depending on the dominant scattering mechanism and the shape of the energetic bands of the semiconductor.[12–16] Furthermore, $r = 1$ for a degenerate semiconductor or high magnetic field ($\mu B \gg 1$). As $r$ is typically unknown, a "Hall mobility" (and accordingly "Hall carrier density") is defined by choosing $r = 1$. This convention is also used throughout this paper. Furthermore, we shall neglect the thickness $d$ of the sample, as it cancels out throughout the calculations. The analysis then yields the sheet resistance $R_s = \rho/d$ and sheet carrier density $n_s = nd$ instead of the resistivity $\rho$ and (bulk) carrier density $n$.

Van der Pauw realized that Hall effect measurements are not restricted to rectangular samples, but can be extended to samples of arbitrary shape as long as the contacts are small and at the edge of the sample, and the sample layer is homogeneous, of uniform thickness, and free of (geometrical) holes.[2,3] This dramatically simplifies the sample preparation, as no micro-structuring of the sample is required. Especially for the analysis of solar cell absorbers this is of great importance, as many labs do not have access to the equipment required for precise Hall bar preparation. A qualitative sketch of a typical specimen according to van der Pauw is shown in Fig. 1(b). Although the current stream lines are no longer necessarily parallel to the sample edges, the same Hall voltage as in Eq. (1) is obtained by integrating the Hall field perpendicular to the current stream lines [solid line between points P and N′ in Fig. 1(b)]. However, if the voltage probes at points P and N are not on the same equipotential line, an additional offset voltage [dashed line between points N′ and N in Fig. 1(b)] will be measured in addition to the magnetic-field-dependent Hall voltage. For measurements on typical solar cell absorbers, this "misalignment voltage" actually poses a tremendous challenge, and will be addressed separately in Sec. III below.

### A. Resistivity

For typical rectangular samples, as shown in Fig. 1(b), the resistance measured along the "length" (current through contacts M and P, voltage measured between N and O, or vice versa) will be different from the resistance measured along the "width" of the sample (current through contacts N and M, voltage measured between O and P, or vice versa). Van der Pauw demonstrated[2] that two such distinct resistances $R_a$ and $R_b$ also exist for a sample with arbitrary shape, and that these resistances are related to the sheet resistance of the specimen by the following equation:

$$\exp\left(-\pi\frac{R_a}{R_s}\right) + \exp\left(-\pi\frac{R_b}{R_s}\right) = 1. \tag{3}$$

The sheet resistance can thus be obtained from the measured values of $R_a$ and $R_b$ along the different sides of the sample by solving Eq. (3) numerically, or by using

$$R_s = \frac{\pi}{\ln 2}\frac{R_a + R_b}{2}f, \tag{4}$$

with tabulated values for the numerical factor $f$,[17] which only depends on the resistivity ratio $R_a/R_b$.

### B. Hall voltage

In van der Pauw configuration [see Fig. 1(b)], the Hall voltage is measured along the diagonals of the sample (current through contacts M and O, voltage measured between N and P, or vice versa). This, however, assumes an ideal sample, which is a perfectly symmetric square of homogeneous material at a constant temperature, and has infinitesimally small ohmic contacts. For a non-ideal sample, the measured transversal voltage $V_m$ along the diagonals is not identical to the Hall voltage $V_H$. On the one hand, thermoelectric effects due to thermal gradients in the probe leads might produce a constant offset voltage $V_0$, which is independent of the applied current or the resistivity of the sample. On the other hand, as discussed earlier, a misalignment voltage is observed if the sample is not perfectly symmetric or the contacts are not identical. This misalignment voltage originates from a potential drop between the two voltage probes, and is, hence, proportional to the applied current and sample resistivity. A more elaborate treatment of the misalignment is given below. The experimentally measured voltage then reads

$$V_m = IR_s(\mu B + \alpha) + V_0, \tag{5}$$

where $\alpha$ is a geometrical factor that converts the sample resistivity to an effective resistance between the Hall voltage probes. The Hall coefficient, and thus the carrier concentration is then calculated according to Eq. (1). Note that a correction for the offset terms $\alpha$ and $V_0$ is typically required, which will be discussed in the following.

### C. Conventional measuring standard for the Hall voltage

As only the Hall voltage $V_H = IR_s\mu B$ is a function of both current and magnetic field in Eq. (5), offsets are usually corrected by reversing the direction of current flow and magnetic field during the measurement.[17]

For each pair of current contacts, the voltages $V_m(+I)$ and $V_m(-I)$ between the Hall voltage probes are measured with a forward and reverse current, respectively. Constant offsets $V_0$ are then eliminated using

$$V^* = \frac{1}{2}\left[V_m(+I) - V_m(-I)\right]. \tag{6}$$

Thermoelectric offsets are commonly small, and the measurement current can be chosen to ensure $V^* \gg V_0$. Hence,

this correction rarely poses a problem, and we will implicitly assume in the following that all measurements have been corrected in this way.

In the conventional measuring standard, the same argument is chosen to eliminate the offset voltage due to misalignment; subtracting two measurements with the magnetic field in opposite directions should allow to isolate the Hall voltage $V_H$ according to

$$V_H = \frac{1}{2}\left[V^*(+B) - V^*(-B)\right]. \tag{7}$$

In fact, van der Pauw in his original work suggested to subtract the voltage measured between the Hall voltage probes without magnetic field from the measured Hall voltage under magnetic field $B$, i.e., $V_H = V^*(B) - V^*(0)$. Conceptually, both approaches are identical in finding the slope of the magnetic-field-dependent voltage $V_m(B)$ from two known values at magnetic fields of either $+B$ and $-B$ (magnetic field reversal), or 0 and $B$ (zero-field offset subtraction). These corrections yield reliable results if $\mu B \gtrsim \alpha$ and if all sample parameters remain constant for all measurements at different magnetic fields. One obvious solution that is presented here to improve the sensitivity of the correction is a sweep of the magnetic field. This allows a fit of the magnetic-field-dependent voltage $V^*(B)$, which significantly reduces the uncertainty compared to relying on only two data points.

### D. Measurement challenges in low-mobility films

It is often stated that Hall measurements should be easiest for low or moderate doping concentrations due to the corresponding large Hall coefficient. For a given measurement current through the sample, the magnitude of the Hall voltage is indeed determined by the Hall coefficient $R_H$, and thus inversely proportional to the carrier density [compare Eqs. (1) and (2)]. This relation suggests that a low or moderate carrier concentration ensures accurate Hall measurements. This argument, however, neglects that the measurement current is limited by the total sample resistance, due to the voltage limitation of the measurement equipment. Consequently, the measurement current has to be adjusted for a low-mobility specimen to keep the driving voltage within sensible limits, and the Hall voltage decreases accordingly.

If we assume that the total sample resistance is proportional to the resistivity (which obviously neglects contact resistances, but remains approximately valid for many material systems where the contact resistance improves with the dopant concentration), the magnitude of the Hall voltage for a given experimental setup is determined by the product $\mu B$. Hence the analysis of a Hall measurement becomes challenging for low-mobility materials, independent of the magnitude of the Hall coefficient, due to experimental limitations on the measurement current. Only for well-conducting samples difficulties due to a small Hall coefficient arise, as the measurement current cannot be increased further due to experimental limitations or in order to limit ohmic sample heating. Most importantly, the signal to noise ratio in the measurement according to Eq. (5) is given by the product $\gamma = \mu B$ in relation to the misalignment factor $\alpha$ or variations in the

sheet resistance $R_s$. Hence, Hall measurements of low-mobility samples are difficult to interpret without a careful correction of the misalignment offset.

In addition to the detrimental impacts of a small measuring current, a high resistance might also require substantial settling times to achieve a stable reading of the measured Hall voltage. Drifts in sample parameters due to an inaccurate temperature stabilization also tend to be more common in highly resistive samples, where typically, either the carrier concentration or the mobility show a thermally activated behavior.

Polycrystalline thin film absorbers for photovoltaic application are a prime example for the challenges of accurate Hall measurements. A review of this topic is given in Ref. 18. Typical solar cell absorbers exhibit moderate carrier concentrations in the range of $10^{15}$–$10^{17}\,\mathrm{cm}^{-3}$, which correspond to fairly high Hall coefficients in the range of $10^4$–$10^2\,\Omega/\mathrm{T}$ for thin films with a thickness of about 1 $\mu$m. The sheet resistance of these polycrystalline thin films, however, can be very high due to the moderate carrier concentration, the small film thickness, and a low carrier mobility due to the presence of grain boundaries. Furthermore, the sheet resistance typically decreases towards lower temperatures due to the semiconducting behavior (reduced carrier concentration at low temperature) and transport barriers (reduced mobility at low temperature). Transparent conductive oxides (TCO) as front window layers, on the other hand, are highly doped but exhibit small grains with low effective mobilities. Besides these fundamental considerations, technological limitations present further challenges; contacts cannot be annealed—and hence need to be made larger—in order to avoid modifications to the absorber during annealing, the study of degradation mechanisms requires the fabrication of degraded—and hence more unstable and challenging—specimen, and persistent photoconductivity might lead to instabilities of the sample that last for days.

Although material systems related to photovoltaic thin-film applications are used as examples in this paper, the results can be equally applied to any other material.

## III. CORRECTION OF THE MISALIGNMENT OFFSET

The misalignment factor $\alpha$ plays a central role in the interpretation of Hall measurements on low-mobility materials. If $\mu B \ll \alpha$ within the range of magnetic fields accessible in the experiment, most measurements will be unreliable or outright meaningless without suitable offset correction. According to Eq. (5) the challenge is to separate a small Hall response—proportional to $\mu B$—from the misalignment offset proportional to $\alpha \gg \mu B$.

First, we will present a general description of misalignment in non-symmetric samples for the ideal case of a homogeneous film with infinitely small contacts at the sample edge, where we assume that $\alpha$ and $R_s$ are constant. We then relax these constrains by first allowing variations of the sheet resistance, and then also allowing variations in the misalignment factor $\alpha$.

## A. Conventional approach

If the sample is not symmetric, the Hall voltage probes without magnetic field will not be at the same potential, and a finite offset voltage $V_{c,d}(B = 0\,\mathrm{T}) \neq 0$ is measured between both probes. The subscripts "c" and "d" denote that the Hall voltage might be measured along either of the two diagonals of the sample; in Fig. 1(b) the current could be passed either through contacts M and O, or through N and P, with voltage being measured between the two remaining contacts in each case. Note that for identical infinitely small contacts $V_c = -V_d$ at $B = 0\,\mathrm{T}$ due to symmetry considerations. The offset voltage results from the potential drop between the voltage probes caused by a current flowing through the specimen with sheet resistance $R_s$, and will, hence, be proportional to $IR_s$. Hence, with the proportionally factor $\alpha$ we obtain

$$R_{c,d} = \frac{V_{c,d}}{I} = R_s(\mu B + \alpha_{c,d}), \tag{8}$$

which is identical to Eq. (5) after eliminating the (current-independent) thermoelectric offset voltage $V_0$ and dividing by the current $I$ (Here we regard the effective Hall resistance $R_{c,d}$ rather than the Hall voltage $V_{c,d}$, as the former is independent of the choice of measurement current).

It is helpful to note that the misalignment factors $\alpha_c$ and $\alpha_d$ of the two different diagonals C and D of a specimen are not independent. For identical infinitely small contacts, the identity $V_c = -V_d$ also implies $\alpha_c = -\alpha_d$. Hence, if the Hall coefficient is determined by averaging both diagonals, the offset voltage due to misalignment is already largely eliminated. Albeit useful, this approach alone is often insufficient:

- In order to obtain accurate and consistent results, it is mandatory to obtain the carrier mobility separately from measurements along each of the sample diagonals. It is not possible to assess the validity of the analysis if the individual measurements are not meaningful. By relying on the average value, one loses a powerful tool to verify the integrity of the measurement.
- As a consistency check, measurements are commonly rejected if the results for two equivalent sides, e.g., the two opposite sides of the sample or the two diagonals differ by more than a certain threshold.[17] Even if averaging both diagonals would yield the correct result, the corresponding data might be discarded as the individual measurements differ by twice the misalignment voltage.
- For non-ideal samples, the misalignment voltages along both diagonals might no longer be equal in magnitude. In a large number of measurements, we empirically found that the difference $\Delta a = |\alpha_c| - |\alpha_d|$ in the absolute values of $\alpha_c$ and $\alpha_d$ is small for typical sample geometries, but could be significant for low-mobility material where $\mu B \ll \alpha$, and thus possibly $\mu B < |\Delta a|$.

According to Eq. (8), as described above, the carrier mobility can be separated from the misalignment offset by taking into account several measurements at different values of the magnetic field, e.g., by reversing the direction of the magnetic field. These procedures, however, implicitly

assume that the sheet resistance $R_s$ and the misalignment factor $\alpha$ are constant in time and independent of temperature during the course of the measurement. For low-mobility material, however, the task is to detect small changes in the measured voltage with a change of magnetic field, and any variation in any of the parameters in Eq. (8) can potentially lead to an erroneous offset correction. Consider, for example, a slight variation of sample temperature, which will cause a variation of the resistivity due to small changes in carrier concentration or mobility. Such a variation, maybe of a few percent in the electrical parameters, is negligible, compared to typical measurement uncertainty. The corresponding relative variation of sample resistance might, however, be easily comparable to or larger than the signal term $\mu B$, completely invalidating the offset correction. One such example is shown below in Sec. IV, where slight temperature variations of fractions of a Kelvin persist for approximately one hour and significantly perturb the Hall signal. Furthermore, magnetoresistance leads to a magnetic-field-dependent resistivity, and hence, poses the same challenges.

### B. Allowing variations in sheet resistance

The time required to measure all 12 contact combinations (4 sides and 2 diagonals, in 2 polarities each) in the van der Pauw technique at a single magnetic field is obviously much shorter than the time required to perform these measurements at several magnetic fields. Hence, in a first approximation, we assume that the sample resistivity is stable for one set of measurements at a given magnetic field. In this case, the normalized effective Hall resistance

$$\frac{R_{c,d}}{R_s} = \mu B + \alpha, \qquad (9)$$

with the magnetic-field dependent sheet resistance $R_s$ according to Eq. (3), evaluated at each magnetic field $B$, is independent of the measurement condition and ideally yields a straight line as a function of magnetic field $B$ if $\alpha$ is constant.

### C. Generalized correction scheme

Fundamentally, the misalignment offset originates from the asymmetry of the potential distribution within the specimen. This asymmetry is predominantly given by the geometric shape of the sample, and the misalignment factor $\alpha_{c,d}$ is constant. If we allow slight inhomogeneities or contacts of finite size, which will partly shunt the sample, the potential distribution within the sample will differ from the ideal case. Hence the "electric shape" of the sample might no longer correspond to the geometric shape, and furthermore might change as a function of the sample sheet resistance. Accordingly, also the misalignment factors $\alpha_c$ and $\alpha_d$ might change with sheet resistance, and thus might no longer be constant during the measurement. The asymmetry of the potential distribution is also the reason why the sample resistivity has to be calculated according to Eq. (3), and why the two resistances $R_a$ and $R_b$ measured along different sides of the sample are, in general, not equal. Specifically, the resistances $R_{c,0}$ and $R_{d,0}$ measured along the different diagonals

of the sample without contribution of the Hall voltage ($B = 0\,\text{T}$) are related to $R_a$ and $R_b$ by equations[2]

$$R_{c,0} = (R_a - R_b), \quad R_{d,0} = -(R_a - R_b). \qquad (10)$$

This allows us to unambiguously determine the change in Hall resistance due to a magnetic field from measurements at a single value of the magnetic field. Combining Eqs. (9) and (10), and using $R_{c,d,0} = R_{c,d}(B = 0) = \alpha_{c,d} R_s$ for the zero-field Hall resistance, we obtain the carrier mobility from

$$\mu B = \xi_{c,d}, \quad \xi_c := \frac{R_c - (R_a - R_b)}{R_s},$$
$$\xi_d := \frac{R_d + (R_a - R_b)}{R_s}. \qquad (11)$$

In the following, we will refer to the quantities $\xi_c$ and $\xi_d$ as the reduced Hall resistances. In Eq. (11) all quantities required to obtain the mobility are directly measured, and we no longer need to determine the unknown misalignment factor $\alpha$. Furthermore, the misalignment factor has thus been related to its physical origin, and Eq. (11) automatically accounts for any instability in some of the sample parameters.

By making use of the zero-field equations, however, we have neglected that the sample resistivity might increase with magnetic field due to magnetoresistance. The individual resistances $R_a$ and $R_b$ do not necessarily change exactly proportional to $R_s$ due to the factor $f$ in Eq. (4), and any variation in $f$ introduces a small error in the offset correction using Eq. (11). For most low-mobility materials this effect is small, but we indeed find that pronounced magnetoresistance can invalidate our approach, as shown in Sec. V for the case of multicarrier conduction. Furthermore, by assuming that $\xi_c$ and $\xi_d$ yield the same mobility, we have still assumed that $\alpha_c = -\alpha_d$ holds true. In reality, we empirically find small deviations between both factors. Then, $\xi_c$ and $\xi_d$ in Eq. (11) are no longer equal and produce two distinct lines with a certain offset if plotted against the magnetic field B, as exemplified by the data in Fig. 2(c). Typically, both slopes are similar and the correct mobility value is still obtained from either of the two lines. Should both lines yield different slopes we suggest that the data be discarded, as the sample will be truly unsuited for a Hall effect measurement in a van der Pauw geometry.

### D. Comparison between the different correction schemes

Figure 2 compares the three different approaches to offset correction discussed above, Eqs. (8), (9), and (11), using the example of a polycrystalline Cu(In,Ga)Se$_2$ thin film, which has been mechanically detached from the conductive growth substrate (Mo-coated glass) for Hall measurements. Due to the presence of grain boundaries, and possibly due to damage inflicted during detachment of the film, the effective Hall mobility is significantly reduced compared to single crystal material, as discussed in Sec. V. As a further complication, the sample resistivity is not perfectly stable, and we observe an increase in resistivity with time even after
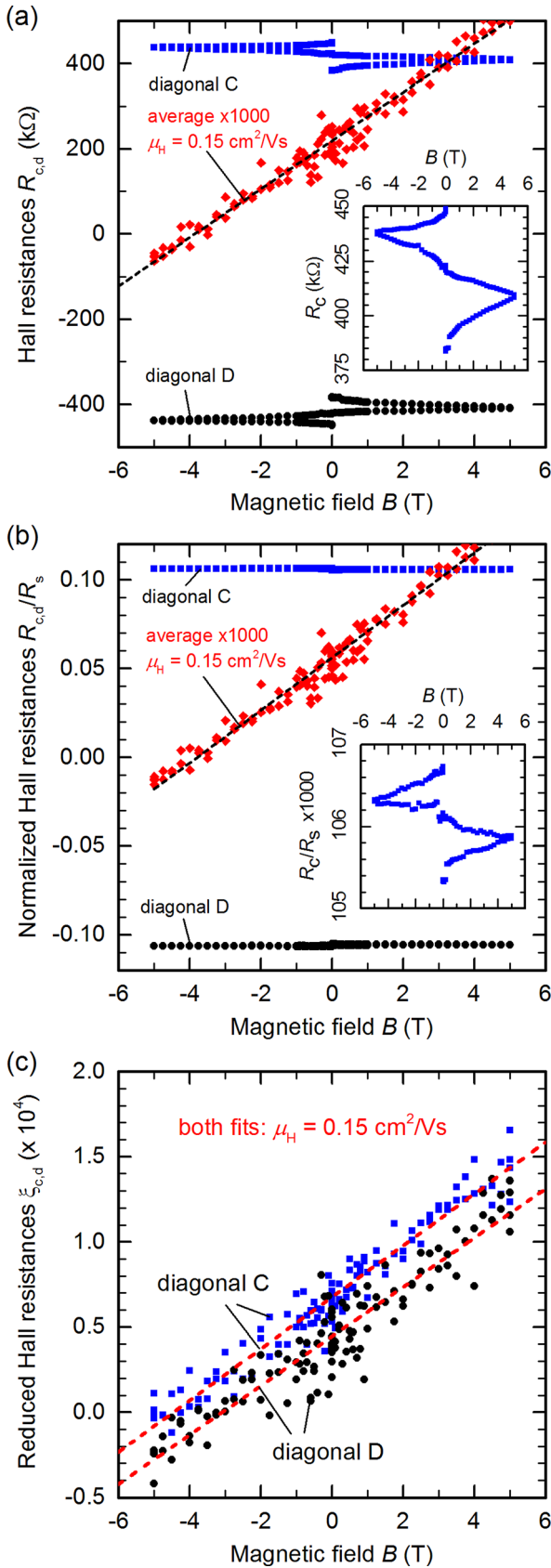
FIG. 2. Comparison of different offset correction schemes. (a) Hall resistance $R_{c,d}$, Eq. (8), (b) normalized Hall resistance $R_{c,d}/R_s$, Eq. (9), and (c) reduced Hall resistance $\xi_{c,d}$, Eq. (11), for both diagonals (blue squares and black circles), respectively. The averaged values are shown in parts (a) and (b) scaled by a factor of 1000. The insets show a magnification to illustrate the magnetic field dependence of $R_c$ and $R_c/R_s$. Dashed lines are fits to the respective data, yielding the same Hall mobility of $\mu_H = 0.15\,\mathrm{cm^2/(V\,s)}$ in all three cases.

keeping the sample in the dark for several days before starting the measurement. Under these circumstances it is crucial to obtain the mobility from a linear fit to the magnetic-field-dependence of the respective quantity—$R_{c,d}$, $R_{c,d}/R_s$, or $\xi_{c,d}$ for the different models—over a wide range of magnetic fields. Using a field-reversal technique, i.e., calculating the mobility from two Hall measurements at positive and negative magnetic field, fails to provide sensible results due to the large offset voltages, temperature variations, and drift in the sample parameters with time.

The conventional approach according to Eq. (8), which is also used in the standard field-reversal technique,[17] is shown in Fig. 2(a) for a range of magnetic fields between $-5\,\mathrm{T}$ and $+5\,\mathrm{T}$, where the sweep direction of the magnetic field was varied ($0\,\mathrm{T} \to +5\,\mathrm{T} \to -5\,\mathrm{T} \to 0\,\mathrm{T}$). The individual measurements along both diagonals C and D do not show a clear trend with magnetic field. Instead, the resistances mirror the evolution of the sheet resistance over time, which hides any magnetic-field-dependent Hall contributions. This is immediately apparent from the "zig-zag" shape of $R_{c,d}(B)$ for the experiment shown here, as without any drift all measurements at a given magnetic field, e.g., $B = 0\,\mathrm{T}$, would yield the same resistance. For a single sweep direction, however, the time dependence of the resistivity could erroneously be interpreted as an apparent magnetic field dependence of the Hall resistance. For example, the inset in Fig. 2(a) clearly suggests a nearly linear magnetic field dependence of $R_{c,d}(B)$ for the sweep from $+5\,\mathrm{T}$ down to $-5\,\mathrm{T}$. Due to the opposite sign of $\alpha_c$ and $\alpha_d$, a linear fit would then yield a different sign for both slopes, suggesting p-type conductivity along one diagonal, and n-type conductivity along the other diagonal (in less extreme cases, the same conductivity type with two different values for the Hall mobility for both diagonals would be obtained). This is further proof that the changes in the measured resistances are not related to the Hall effect. If both diagonals are averaged, however, the misalignment offsets largely cancel and we obtain a linear magnetic-field-dependence of the Hall resistance corresponding to an effective Hall mobility of $\mu_H = 0.15\,\mathrm{cm^2/(V\,s)}$, red diamonds in Fig. 2(a), consistent with both other models discussed below. Note that the Hall signal is clearly resolved despite the low magnitude of the Hall voltage, which is only $\approx 0.1\%$ of the measured voltage including offsets (the averaged Hall resistance in Fig. 2(a) is scaled by a factor of 1000).

Correcting for variations of the sheet resistance according to Eq. (9), as shown in Fig. 2(b), yields nearly constant values of $R_{c,d}/R_s \approx \alpha_{c,d} \approx \pm 0.1$, again corroborating that the Hall voltage is small compared to the offset value. As expected, the normalized Hall resistance is less sensitive to variations in the sheet resistance ($R_c/R_s \approx 0.105$–$0.107$ in this experiment, a variation of $+1.5\%$ relative) compared to the Hall resistance ($R_c = 375$–$450\,\mathrm{k\Omega}$, $+20\%$ relative). Nevertheless, a closer look at $R_c/R_s(B)$, shown in the inset of Fig. 2(b), still does not yield a linear dependence on magnetic field. Accordingly, for this particular sample, this correction scheme is still insufficient to obtain the carrier mobility, as small variations of $\alpha_c$ and $\alpha_d$ are still larger than the Hall signal $\mu B$. The average value of both diagonals, however, again yields a linear

magnetic-field-dependence corresponding to $\mu_H = 0.15 \, \text{cm}^2$ /(V s). Note that we have chosen a particularly challenging sample for this example. The offset correction scheme according to Eq. (9) would in fact be suitable for slightly higher mobilities of a few $\text{cm}^2$/(V s), as the Hall signal $\mu B$ would then no longer be obscured by the small variations in $\alpha_{c,d}$.

Finally, the offset correction based on the reduced Hall resistance $\xi_{c,d}$ according to Eq. (11) shown in Fig. 2(c) yields straight lines for both diagonals, which both correspond to the same Hall mobility of $\mu_H = 0.15 \, \text{cm}^2$/(V s). Non-idealities in the misalignment are apparent here from the offset between both lines and from $\xi_{c,d}(B = 0 \, \text{T}) \neq 0$.

Although the same Hall mobility of $\mu_H = 0.15 \, \text{cm}^2$/(V s) is obtained for all three correction schemes—when averaging both diagonals—only Eq. (11) produces meaningful results for each of the individual diagonals for this sample, and thus allows to verify the consistency of the obtained results. Furthermore, due to large scatter in the data typical for low-mobility films, the analysis is only possible if a large number of measurements at different magnetic fields are taken into account.

In order to explore the limit of Eq. (11), Fig. 3 shows the reduced Hall resistances for a Hall measurement of a non-intentionally-doped $CuCrO_2$ transparent conductive thin film[19] at a sample temperature of 270 K. Despite large scatter in the data, the $p$-type conductivity at a mobility of the order of $10^{-2} \, \text{cm}^2$/(V s) is still resolved.

## IV. TEMPERATURE CORRECTION AND STABILIZATION TIME

Although misalignment offsets can be corrected for in most cases, as shown above, a more fundamental understanding of the influence of different measurement conditions on
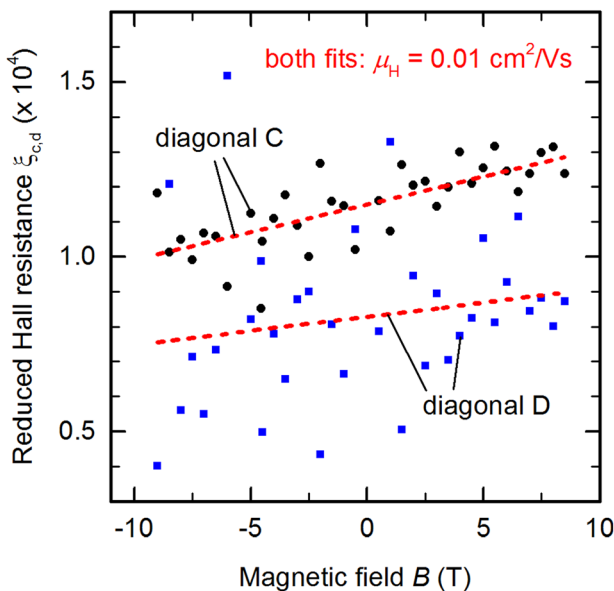
the raw data is necessary for an accurate interpretation of measurement results.

Due to their large influence on the measurement, variations in the sheet resistance deserve close attention. Figure 4 shows a continuous measurement of the longitudinal resistance $R_a$, required to calculate the sheet resistance, along one sample edge (black solid line) while the magnetic field (red dashed line) is swept in three distinct steps from 0 T to –5 T. Well defined steps in the resistance as a result of magnetoresistance are observed when changing the magnetic field, but the signal appears to lag behind the magnetic field within a time interval of nearly one hour. The same behavior is observed for all contact configurations, as the measured resistances are all proportional to the sheet resistance. Consequently, an incorrect Hall resistance would be measured if the specimen was not allowed sufficient time to stabilize. The substrate temperature recorded during the measurement is shown by the blue line in the upper part of Fig. 4, and shows a striking correlation with the deviations of the measured resistance from the expected trend. This becomes evidently clear when looking at a small disturbance 3.5 h after the start of the measurement (produced by gently tapping onto the clamp holding the probe stick; earlier perturbations are caused by heat dissipation in the magnet during ramping of the magnetic field).

To illustrate the influence of the sample temperature, the gray line in Fig. 4 shows an empirically temperature-corrected resistance. This empirical correction is obtained from a fit to the temperature-dependent stabilized resistance without magnetic field (not shown here) for a small temperature variation around the nominal setpoint. For this particular sample, we find that the sheet resistance changes by 0.5% relative per degree temperature deviation from the setpoint. The temperature-corrected resistance then shows the expected behavior and nearly instantaneously follows the



FIG. 3. Limiting case for the offset correction according to Eq. (11) for Hall measurements of a non-intentionally-doped $CuCrO_2$ thin film. The linear fits yield a $p$-type conduction with a mobility of the order of $10^{-2} \, \text{cm}^2$/(V s).
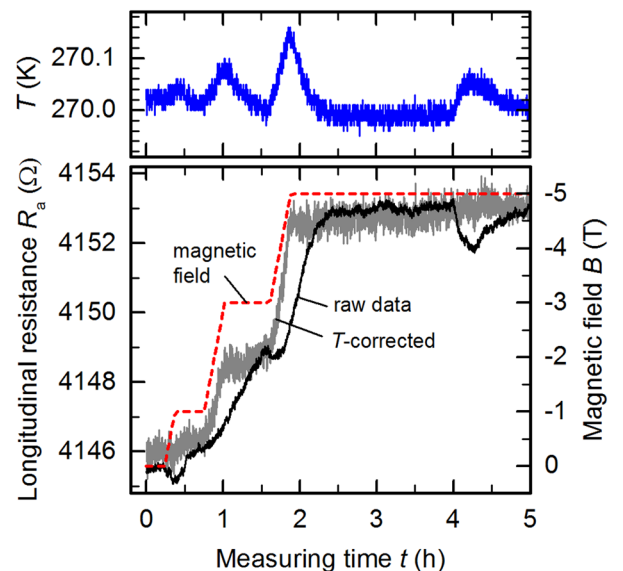


FIG. 4. Measurement of magnetoresistance of an artificially degraded polycrystalline ZnO film. (top) Substrate temperature and (bottom) measured (black solid line) and temperature-corrected (gray solid line) longitudinal resistance $R_a$ along one sample edge (left axis) and the magnetic field (red dashed line, right axis) as a function of time.
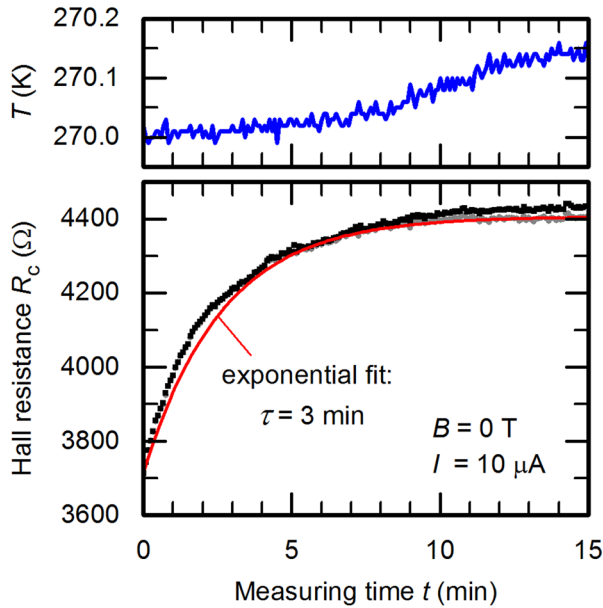
FIG. 5. (top) Substrate temperature and (bottom) measured (black squares) and temperature-corrected (gray circles) diagonal resistance $R_c$ without magnetic field as a function of measuring time $t$. A source current of $10\,\mu A$ is applied to the sample at $t = 0$. The red line is an exponential fit to the temperature-corrected resistance and yields a time constant of 3 min.

change in magnetic field. Note that the temperature spikes in this example are in a range of only 30–160 mK. They nevertheless have a tremendous impact on the measurement due to the small differences in resistance being measured here, which are less than 0.2% of the total resistance. This further serves to highlight that the assumption of a constant sheet resistance in the Hall analysis is rarely valid if a measurement resolution of the order of fractions of a percent is required for offset correction, as might often be the case when studying photovoltaic materials.

In the example of Fig. 4, the delayed response of the resistance to a change in magnetic field was fully explained by the difference in sample temperature. In some cases, however, sufficient time for equilibration of current flow through the sample is required independent of sample temperature. Figure 5 exemplarily shows the evolution of measured resistance (here: resistance $R_c$ along one sample diagonal, without magnetic field) as a function of time $t$ for a polycrystalline Cu(In,Ga)Se$_2$ thin film grown on a glass substrate. The measurement current is switched on at $t = 0$, and then kept constant at $I = 10\,\mu A$ for 15 min. In this particular example, it takes more than 10 min for the resistance readings to stabilize, which is well described by an exponential saturation $R_c = R_0 + \Delta R[1 - \exp(-t/\tau)]$ with a time constant of $\tau = 3$ min. Unlike the previous example shown in Fig. 4, the sample temperature is virtually constant during the initial saturation, and correcting for temperature variations only slightly influences the saturation value due to a warming of the sample by +0.15 K. Hence, instabilities in the sample temperature cannot account for the measured resistance transient.

Such a significant stabilization time after switching the contact configuration in the measurement jeopardized one of the fundamental procedures in a Hall measurement

according to the van der Pauw method; each measurement at a single magnetic field requires 12 individual measurements in different contact configurations (4 sides and 2 diagonals, each measured with two opposite directions of current flow). For a settling time of 10 min, this translates to a total measurement time in excess of two hours for the measurements at a single magnetic field. This makes it exceedingly difficult to acquire a sufficient number of data points at stable experimental conditions for a statistically meaningful analysis.

The technique of continuously monitoring the resistance along one chosen direction, as presented in Figs. 4–6, is a useful tool when measuring unstable samples or samples requiring large settling times. The Hall voltage is only measured along one diagonal of the sample, hence keeping the contact configuration the same without interrupting current flow. The Hall voltage is then continuously measured, which allows a direct real-time assessment of the stability of the measurement. After stabilization, the magnetic field is changed in several steps, each time allowing sufficient time for stabilization of the Hall response and—depending on the scatter in the measured voltages—a sufficiently large time interval to perform an averaging of the Hall voltage at each value of the magnetic field. The sheet resistance, which is required to calculate the carrier mobility, can be determined separately before and after the measurement of the Hall voltage. Separating the measurements of Hall coefficient and sheet resistance is far from ideal, but the drawbacks can be mitigated somewhat:

- Repeatedly increasing and decreasing the magnetic field allows to verify that changes in the measured Hall voltage are indeed related to the Hall effect, if the same Hall voltage is obtained for a given magnetic field at different times in the measurement cycle.
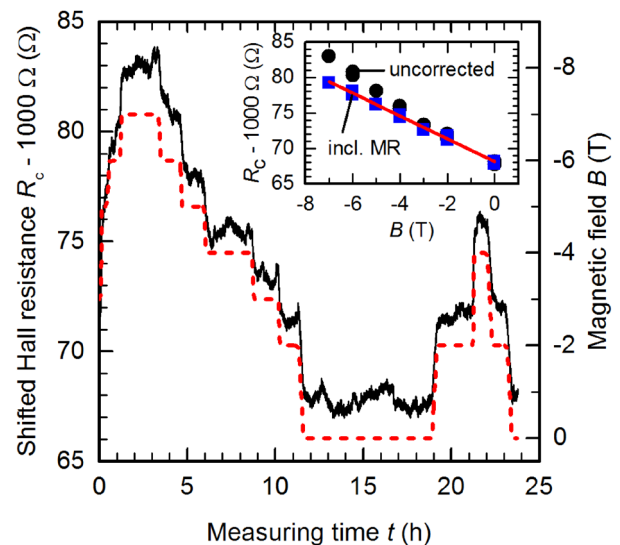


FIG. 6. Shifted Hall resistance $R_c - 1000\,\Omega$ (black solid line, left axis) and magnetic field $B$ (red dashed line, right axis) as a function of measuring time $t$. The inset shows the average Hall resistance for each magnetic field (black circles: uncorrected; blue squares: corrected for magnetoresistance). The red solid line is a linear fit corresponding to a carrier concentration of $n \approx 10^{19}\,cm^{-3}$ and mobility of $\mu_H \approx 1\,cm^2/(V\,s)$.

- After stabilization of the Hall voltage, variations of the sheet resistance can be identified from drifts in the Hall voltage at constant magnetic field. Together with direct measurements of the sheet resistance before and after the measurement this allows to quantify the corresponding measurement uncertainty.

- If the sheet resistance is in principle stable, but varies due to magnetoresistive or temperature-related effects, this can be accounted for by a separate continuous measurement of the magnetic-field-dependent longitudinal resistance along one sample edge, comparable to the measurement shown in Fig. 4.

An example of such a continuous Hall measurement is shown in Fig. 6 for an artificially degraded polycrystalline ZnO film (the same sample as in Fig. 4), where the continuous monitoring allowed to average over the fluctuations in the Hall voltage. The inset shows the resulting average values of the Hall resistance at each magnetic field. In order to correct for the magnetoresistance, these values were divided by $\rho(B)/\rho_0 = 1 + (0.0084\,\mathrm{T^{-1}}B)^2$, which was obtained from a separate measurement of the magnetic-field dependent sheet resistance (a part of this measurement is shown in Fig. 4). This magnetoresistance in the ZnO film is attributed to its polycrystalline nature, as discussed in Sec. V.

Continuously monitoring the Hall voltage at different magnetic fields is equally useful if an unambiguous offset correction is not possible, for example if measurement uncertainties or transients in the sample parameters do not allow to compare consecutive measurements under different contact configurations (Note that all offset correction schemes presented above require several measurements, Eq. (11) requires $R_{c,d}$ along at least one diagonal as well as $R_a$ and $R_b$, and Eqs. (8) and (9) require measurements at different magnetic fields). However, a continuous monitoring obviously fails if offsets become exceedingly large compared to the Hall signal, and defined steps in the Hall resistance are no longer resolvable when changing the magnetic field.

## V. GRAIN BOUNDARIES AND MULTI-CARRIER CONDUCTION

The preceding discussion focused on the challenge how to accurately measure low mobility samples, without addressing the reason for a low mobility in the first place. This section discusses two common mechanisms, grain boundaries and multiple carrier species, that result in an apparent Hall mobility which could underestimate the actual mobility of the charge carriers by several orders of magnitude.

### A. Hall mobility of polycrystalline semiconductors

The original proof of the van der Pauw technique by conformal mapping is based on the assumption of a homogeneous conductor. In common thin film photovoltaic devices, however, all active layers are preferably deposited by low-cost processes, and are hence typically not single-crystalline. Due to the presence of grain boundaries, polycrystalline thin films can no longer be regarded as laterally homogeneous conductors, and care must be taken in the interpretation of

Hall measurement on such films. In the following, we shall assume an idealized polycrystalline semiconductor represented by homogeneous grains separated by grain boundaries much thinner than the average grain size. In particular, we demand that dopant concentration and mobility are homogenous inside each grain, and are the same in every grain. Furthermore, we shall assume that the grain boundaries act as potential barriers, hence impeding current flow. For these conditions, calculations by various authors[18,20–24] show that valuable information about the transport properties of the specimen can still be obtained for polycrystalline films.

In simplified terms, the effective Hall coefficient of such a polycrystalline specimen is mainly given by the in-grain Hall coefficient, if the grain boundaries are assumed to be depleted (i.e., less conductive than the grains) and if the transport barrier at the grain boundary is not too large. Accordingly, Hall measurements on polycrystalline material typically yield a fairly reasonable approximation of the in-grain carrier concentration. The true in-grain carrier concentration will be somewhat underestimated, as the in-grain Hall voltage source is connected in parallel to a larger Hall voltage source (larger $R_H$ due to reduced carrier concentration in the depleted grain boundary), and the effective Hall coefficient will exceed its in-grain value.

Even if Hall measurements can provide a fairly accurate estimate of the carrier concentration, the experimental Hall mobility might underestimate the in-grain mobility by several orders of magnitude.[20,21] The Hall mobility $\mu_H$ is obtained from the measured Hall coefficient and resistivity according to Eq. (2), which implicitly assumes that carrier concentration $n$ and mobility $\mu$ are related by $\rho = (qn\mu)^{-1}$. In order to obtain the in-grain Hall mobility from the in-grain carrier density, we hence need to know the in-grain resistivity. Any (macroscopic) resistance measurement, however, yields the total resistance of the whole specimen. For practical sample geometries and typical grain sizes, any current path between two contacts will cross a large number of grain boundaries, which act as resistive barriers to the current flow. Accordingly, the macroscopic resistance will be dominated by the highly-resistive grain boundaries, and the effective macroscopic resistivity will far exceed the in-grain resistivity.

The work of Jerhot and Snejdar[21] provides a set of simple equations to relate the measured effective Hall mobility and carrier concentration to the individual transport properties of the grains and grain boundaries for several important limiting cases. For the case of dominant ohmic transport across the depleted grain boundaries, the ratio of measured effective carrier concentration and mobility with respect to the in-grain values is given by

$$\frac{n_{\mathrm{eff}}}{n_g} = \left[1 + MD + D^2 e^{\phi/kT}\right]^{-1}, \tag{12a}$$

$$\frac{\mu_{\mathrm{eff}}}{\mu_g} = \left[1 + MD e^{\phi/kT}\right]^{-1} + MD, \tag{12b}$$

where $M = \mu_{\mathrm{gb}}/\mu_g$ and $D = d_{\mathrm{gb}}/d_g$ are the mobility $\mu$ and size $d$ of the grain boundary region normalized to the

in-grain mobility and average grain diameter, respectively, and $\phi$ is the potential barrier at the grain boundary (accordingly, the term $e^{\phi/kT}$ is equivalent to the ratio of in-grain and grain boundary carrier concentration). In many cases, the mobility obtained from a Hall measurement will thus appear to be thermally activated at low temperatures.

If both effective carrier concentration and mobility are measured as a function of temperature, the true in-grain carrier concentration and mobility, as well as the barrier height at the grain boundary, can be obtained from a fit of Eq. (12) to the temperature-dependent data. An example is show in Fig. 7, where the effective hole concentration $p$ and Hall mobility $\mu$ obtained by Hall measurements are plotted against the inverse temperature $1000/T$ for a set of three samples: an as-grown Cu(In,Ga)Se$_2$ (CIGS) film grown on glass (black squares), the same sample after deposition of 50 nm of CdS onto the front surface (red circles), and a second absorber grown in the same deposition run on Mo-coated glass, and subsequently, mechanically detached from the conductive substrate (blue triangles).[25]

For simplicity, we assume that the in-grain carrier concentration and mobility are constant with temperature in the small temperature range investigated here. Due to the more
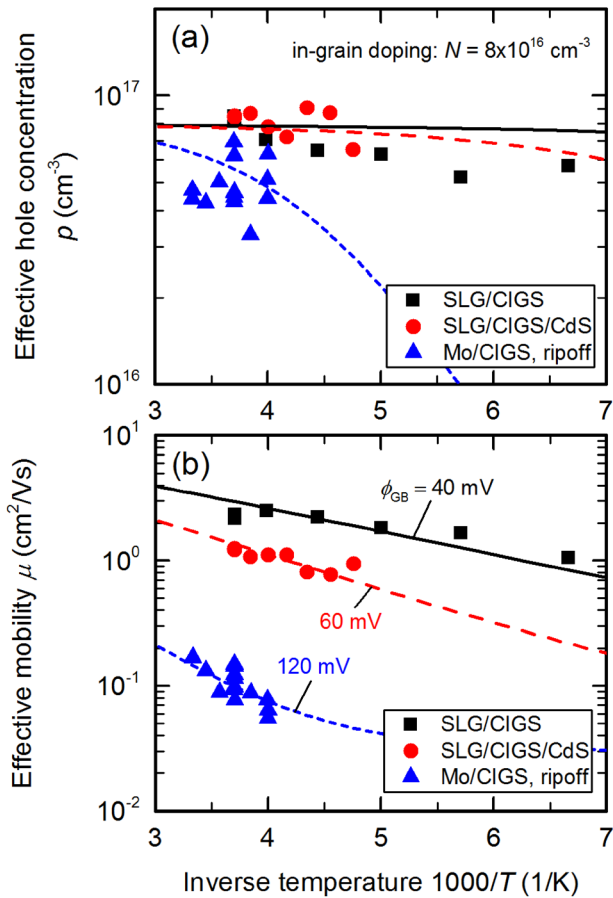


FIG. 7. (a) Effective hole concentration $p$ and (b) Hall mobility $\mu$ obtained by Hall measurements on polycrystalline Cu(In,Ga)Se$_2$ thin films as a function of inverse temperature $1000/T$. Lines are best fits of Eq. (12), which yield $n_g = 8 \times 10^{16}$ cm$^{-3}$, $\mu_g = 30$ cm$^2$/(V s), $\mu_{gb} = 0.9$ cm$^2$/(V s) [0.6 cm$^2$/(V s) for the ripped-off sample], and $d_{gb}/d_g = 0.05$. The barrier height $\phi_{GB}$ at the grain boundary for each sample is given in part (b). Reproduced with permission from Werner *et al.*, Thin Solid Films **633**, 222–226 (2017). Copyright 2017 Elsevier.

pronounced thermally activated behavior in Eq. (12b), the fit is more sensitive to the measured mobility values compared to the carrier concentrations. Thus, the assumption of a constant in-grain carrier concentration explains the bad fit of the hole concentration for the SLG/CIGS sample (black squares) at low temperatures, but beyond that has negligible influence on the extracted transport parameters. The mobility, on the other hand, will typically be only weakly temperature-dependent due to the dominance of defect scattering[26,27] in a mobility range well below 100 cm$^2$/(V s) in CIGS. As only ratios enter in Eq. (12), it is straight forward to implement a model accounting for the temperature-dependence of in-grain parameters, although it does add a number of additional free parameters to the fit.

Lines in Fig. 7 show that all three sets of experimental data are well described by Eq. (12) using the same material parameters for all samples (parameters are given in the caption of Fig. 7). The only difference between the three samples appears to be a different barrier height at the grain boundaries ($\phi = 40$ meV as-grown, 60 meV after CdS deposition, and 120 meV after rip-off), taking into account a slight deterioration of the grain boundary mobility during the rip-off process. Note that even for the as-gown sample on glass, which shows the lowest barrier height of 40 meV at the grain boundaries, the effective mobility obtained from a single Hall analysis at one temperature still underestimates the true in-grain mobility by one order of magnitude.

Equation (12) was derived for ohmic transport across depleted grain boundaries. For thermionic emission or tunneling through the grain boundary Jerhot and Snejdar[21] find instead that

$$n_{\text{eff}} \approx n_g \text{ and } \mu_{\text{eff}} \approx \frac{\mu_g \mu_t}{\mu_g + \mu_t} = \left[\frac{1}{\mu_g} + \frac{1}{\mu_t}\right]^{-1}, \quad (13)$$

where $\mu_t$ is the mobility associated with the thermionic emission or tunneling of the charge carriers through the grain boundary. If emission over the grain boundary limits the macroscopic conductivity, i.e., if $\mu_t \ll \mu_g$, a Hall experiment would thus approximately yield the in-grain carrier concentration and the mobility $\mu_t$ of the grain boundary region.

In principle, the magnetic-field dependence of the measured transport properties might provide further insight to disentangle the transport properties of in-grain and grain boundary domains (see the Appendix). Due to the drastic effect of grain boundaries on the effective mobility, the resulting magnetic-field dependence described by $\gamma = \mu B \ll 1$ is, however, often negligible.

## B. Multi-carrier conduction

Different types of carriers with different polarities or mobility values might be present in a given sample. Typical scenarios for this include, e.g., conduction via defect states parallel to band conduction in a semiconductor, different transport properties in different (parallel) layers of a stacked device, minority carriers in an illuminated or heated semiconductor, etc. In this case, each carrier species adds independently to the sample conductivity, but their respective Hall voltages are

connected in parallel. A Hall measurement will thus yield a weighted average effective mobility, which could become very small if Hall voltages with opposite polarity, i.e., electrons and holes, are both present in sufficient numbers. In the extreme case, for the same number of electrons and holes with equal mobility, the resulting effective Hall mobility will, in fact, be zero independent of the actual mobility of the individual charge carriers. Consequently, a low measured effective mobility alone is not necessarily a convincing indication that the true mobility of the charge carriers is indeed low.

Multi-carrier effects are most readily analyzed in context of the magnetic-field-dependent conductivity tensor (see the Appendix). Note that the same information can be obtained by studying the magnetic-field dependence of sheet resistance (also called magnetoresistance) and Hall resistance, which are the diagonal and off-diagonal components of the resistivity tensor. For low-mobility specimen, the tensor formalism rarely allows to study different charge carrier species in detail, as the magnetic-field dependence is described by the term $\gamma = \mu B \ll 1$, and thus difficult to resolve experimentally. Nevertheless, the conductivity tensor can be helpful to avoid misinterpretation of apparently low mobility values in a given Hall measurement.

As practical example, Fig. 8 shows a typical Hall measurement of a $p$-type epitaxial CuGaSe$_2$ thin film, where electron conduction via defect states presents a second conduction channel at low temperatures, parallel to hole conduction in the valence band. The apparent Hall mobility according to Eq. (8) is shown in Fig. 8(a) and appears to vary by almost three orders of magnitude over the temperature range investigated here. Figure 8(b) shows the corresponding sheet conductivity tensor at a sample temperature of $T = 100$ K. Note the different scale on the x- and y-axes, and that a circular graph in the $\sigma_{xx}$–$\sigma_{xy}$ plane would be expected for single-carrier conduction (see the Appendix). Despite this obvious deviation from a simple single-carrier model, the corresponding Hall resistance $\langle R_{c,d} \rangle$ averaged over both diagonals shows an almost perfectly linear magnetic-field dependence as shown in Fig. 8(c). Taking the linear slope in Fig. 8(c), one would thus obtain an incorrect single-carrier mobility of $\mu_H = 110$ cm$^2$/(V s). In contrast, the individual Hall resistances $R_c$ and $R_d$ along both diagonals prior to averaging, as well as $R_{c,d}/R_s$ and $\xi_{c,d}$ used in Eqs. (9) and (11), indeed deviate from a linear magnetic-field-dependence as expected [$\xi_{c,d}$ shown exemplarily in Fig. 8(d)]. This further emphasizes the importance of consistency checks and highlights the challenges associated with the conventional offset correction according to Eq. (8). Furthermore, even epitaxial samples with majority carrier mobilities likely in a range of a few 100 cm$^2$/(V s) might yield an apparent Hall mobility below 1 cm$^2$/(V s) at conditions where multi-carrier phenomena are significant.

## VI. DISCUSSION AND CONCLUSIONS

Hall measurements form the most important technique in order to directly obtain the charge carrier concentration and mobility of (semi-) conducting specimen. Its wide-spread use as a simple and fast routine measurement technique is certainly also based on the simplicity of the van der Pauw formalism concerning sample preparation.
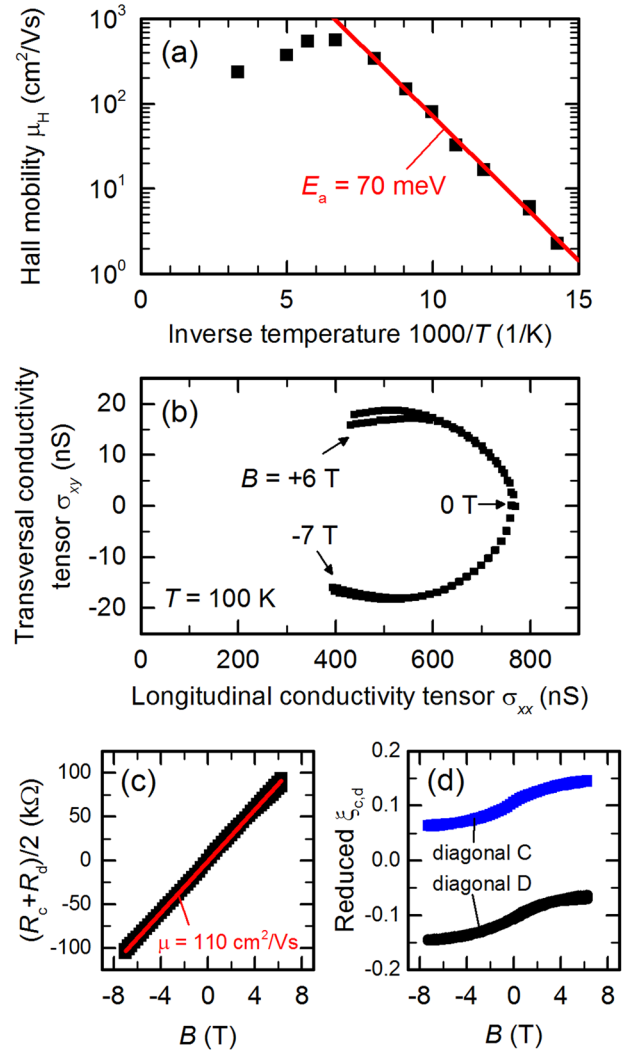


FIG. 8. (a) Temperature-dependent apparent Hall mobility with activation energy $E_a = 70$ meV of an epitaxial CuGaSe$_2$ thin film grown on semi-insulating GaAs. (b) Sheet conductivity tensor plotted in the $\sigma_{xx}$-$\sigma_{xy}$ plane at $T = 100$ K. Corresponding (c) Hall resistance $\langle R_{c,d} \rangle$ averaged over both diagonals and (d) reduced Hall resistance $\xi_{c,d}$ as a function of magnetic field $B$.

For low-mobility materials, offset voltages due to deviations from an ideal sample geometry and resistivity variations due to temperature fluctuations often obscure the small Hall signal, which is proportional to the mobility. As a first step, the measurement resolution can be increased significantly, if a sufficient number of measurements at different magnetic fields is taken into account. As a second step, the chosen model for offset correction can have a strong impact on the data analysis.

Using the conventional standard for offset correction, the apparent Hall voltage typically is not a linear function of applied magnetic field, and the extracted Hall coefficient differs between nominally identical contact configurations, e.g., both diagonals of a rectangular sample. Although averaging of both diagonals might often still yield the correct result, this approach is not reliable without further consistency checks and verification, as was shown in the example of an epitaxial layer showing multi-carrier conduction.

It was shown that offset correction can be significantly improved if variations in sheet resistance with temperature or magnetic field are taken into account by normalizing the

measured Hall resistances with respect to the sheet resistance determined in the same measurement. Nevertheless, for particularly challenging samples this approach might face the same challenge that only averaging of both diagonals yields the desired result, which makes consistency checks impossible and the results ultimately useless.

An improved correction scheme was proposed, where the lateral resistances along the sample edges are used to estimate the actual misalignment factor. In this case, a linear magnetic-field-dependence is typically achieved for both diagonals individually. This method allows to extend the accessible measurement range of dc Hall measurements to mobility values well below $1\,cm^2/(V\,s)$.

The potentially detrimental impact of insufficient stabilization times and even minute temperature variations for highly resistive samples was addressed. The continuous monitoring of the Hall voltage while sweeping the magnetic field was presented as an alternative measurement procedure for samples, where voltage transients over several minutes might extend the measurement time required for a complete van der Pauw analysis to many hours or even days. This monitoring procedure is also useful to account for temperature variations of the sample, if the sample temperature is recorded during the voltage measurement.

Even with a successful offset correction, the mobility values and carrier concentrations obtained from a Hall measurement are often not representative of the "true" material properties, even taking into account deviations of the Hall scattering factor $r$ from unity. In polycrystalline samples, transport barriers associated with grain boundaries violate the implicit assumption that charge carrier concentration and mobility within the grain are related by the measured sample resistivity. If a suitable transport model is available, temperature-dependent measurements allow to disentangle the in-grain properties from the transport barriers at the grain boundaries. As shown in the example of a $Cu(In,Ga)Se_2$ polycrystalline thin film, the in-grain mobility can be underestimated by orders of magnitude even for a fairly low barrier height at the grain boundaries of a few tens of meV.

Furthermore, different ensembles of charge carriers might contribute to conduction, for example due to band/defect conduction or in layered devices. Failure to account for multi-carrier conduction then leads to incorrect results. The magnetic-field-dependent conductivity tensor was shown to be a convenient tool to validate whether a simple single-carrier transport model is applicable in a given experiment.

The practical examples presented here focus on $Cu(In,Ga)Se_2$ thin film solar cells, where many crucial device parameters are difficult to obtain reliably. The discussion however applies equally to any other low-mobility material measured in van der Pauw configuration, and can serve as a useful guide for material scientists to improve the reliability of dc Hall measurements for low-mobility films with mobility values well below $1\,cm^2/(V\,s)$.

## APPENDIX: CONDUCTIVITY TENSOR IN A MAGNETIC FIELD

Electrical transport in a planar sample (located in the $x$-$y$ plane) in the presence of a perpendicular magnetic field $B$ (along the $z$-axis) is described by the conductivity tensor. The tensor formalism can be found in a large number of publications, for example, Refs. [13], [28], and [29], and we only provide a short summary here.

The current density $J$ through the device depends on the electric field $E$ as

$$\begin{pmatrix} J_x \\ J_y \end{pmatrix} = \begin{pmatrix} \sigma_{xx} & \sigma_{xy} \\ -\sigma_{xy} & \sigma_{xx} \end{pmatrix} \begin{pmatrix} E_x \\ E_y \end{pmatrix}. \tag{A1}$$

For a single ensemble of charge carriers with concentration $n$ and mobility $\mu$, the diagonal and off-diagonal components of the conductivity tensor are given by

$$\sigma_{xx} = \frac{\sigma_0}{1+\gamma^2} \text{ and } \sigma_{xy} = \frac{\sigma_0\gamma}{1+\gamma^2} = \gamma\sigma_{xx}, \tag{A2}$$

where $\sigma_0 = nq\mu$ and $\gamma = \pm\mu B$ (positive for holes and negative for electrons). Note that Eq. (A2) describes a circle with radius $\sigma_0/2$ around the point $(\sigma_0/2|0)$ in the $\sigma_{xx}$-$\sigma_{xy}$ plane for a single carrier species. Deviation from a circular graph thus indicates multi-carrier phenomena or inhomogeneities.

Individual conductivity tensors are additive for multiple carrier ensembles: $\sigma_{xx} = \sum_i \sigma_{xx.i}$ and $\sigma_{xy} = \sum_i \sigma_{xy.i}$. Their individual transport properties can be obtained by a fitting procedure.[29] In generalized form, the summation over few distinct carrier species is replaced by integration over a continuous mobility spectrum $s(\mu)$.[30] However, quite elaborate algorithms are required to estimate $s(\mu)$ by mobility spectrum analysis (MSA)[30–34] of the experimental conductivity tensor.

Polycrystalline material can be understood as a multicarrier system as well, where one carrier species represents the in-grain carriers, while transport across the grain boundaries is modelled as a second carrier type. Their respective conductivity tensors are not additive, since consecutive grains along the current path are connected *in series*. Calculating the resulting conductivity tensor is, thus, not straightforward, and we propose a different approach.

We assume a single linear chain of alternating grains and grain boundaries. Each element $i$ (grain, grain boundary, possibly additional interface regions, …) with length $d_i$ is described by its own conductivity tensor $\underline{\sigma}_i$. We demand that the transversal electric field $E_y$ is given by the Hall field $E_H$ everywhere in the sample, and that there is no net transversal current flow, $J_y = 0$. These constraints lead to equation

$$\begin{aligned} J_y &= \sum d_i J_{y.i} = \sum d_i \left[ \frac{\sigma_{xx.i}^2 + \sigma_{xy.i}^2}{\sigma_{xx.i}} E_H - \frac{\sigma_{xy.i}}{\sigma_{xx.i}} J_x \right]_i \\ &= \sum [d_i \sigma_{0.i}] E_H - \sum [d_i \gamma_i] J_x = 0. \end{aligned} \tag{A3}$$

Equation (A1) can be solved to obtain the longitudinal field $E_{x.i}$ in each element as a function of the applied current density $J_x$

$$E_{x.i} = \frac{1}{\sigma_{xx.i}} J_x - \frac{\sigma_{xy.i}}{\sigma_{xx.i}} E_H = J_x \left( \frac{1 - \chi \sigma_{xy.i}}{\sigma_{xx.i}} \right). \tag{A4}$$

For the right hand side, we have used the substitution

$$\chi = \frac{E_H}{J_x} = \frac{\sum d_i \gamma_i}{\sum d_i \sigma_{0.i}} = \frac{\sum d_i \mu_i}{\sum d_i \sigma_{0.i}} B, \tag{A5}$$

which follows directly from Eq. (A3) and is proportional to the effective Hall coefficient of the polycrystalline sample. The total resistivity of the linear chain of grains and grain boundaries is then obtained by summing the potential drop $d_i E_{x.i}$ across each of the elements, which yields

$$\rho = \frac{\sum d_i E_{x.i}}{J_x \sum d_i} = \frac{1}{\sum d_i} \sum \left( \frac{1 - \chi \sigma_{xy.i}}{\sigma_{xx.i}} \right) d_i. \tag{A6}$$

Together, Eqs. (A5) and (A6) describe the magnetic field dependence of the transverse and longitudinal resistivity of the polycrystalline sample.

[1]E. H. Hall, "On a new action of the magnet on electric currents," Am. J. Math. **2**, 287–292 (1879).

[2]L. J. van der Pauw, "A method of measuring specific resistivity and Hall effect of discs of arbitrary shape," Philips Res. Rep. **13**, 1–9 (1958).

[3]L. J. van der Pauw, "A method of measuring the resistivity and Hall coefficient on lamellae of arbitrary shape," Philips Tech. Rev. **20**, 220–224 (1958).

[4]D. M. Rowe and V. S. Shukla, "A sensitive AC system for measuring changes in small hall voltages at high temperatures," IEEE Trans. Instrum. Meas. **33**, 19–21 (1984).

[5]L. R. Tessler, M. Nissim, U. Dai, and R. L. Rosenbaum, "Hall voltage measurements using ac lock-in detection," Rev. Sci. Instrum. **62**, 835 (1991).

[6]N. Z. Lupu, N. M. Tallan, and D. S. Tannhauser, "Apparatus for measuring the hall effect of low-mobility samples at high temperatures," Rev. Sci. Instrum. **38**, 1658–1661 (1967).

[7]O. Gunawan, Y. Virgus, and K. F. Tai, "A parallel dipole line system," Appl. Phys. Lett. **106**, 062407 (2015).

[8]J. Lindemuth and S.-I. Mizuta, "Hall measurements on low-mobility materials and high resistivity materials," Proc. SPIE **8110**, 81100I (2011).

[9]W. N. Shafarman, S. Siebentritt, and L. Stolt, "Cu(In,Ga)Se$_2$ solarcells," in *Handbook of Photovoltaic Science and Engineering*, 2nd ed. (Wiley and Sons, Chichester, UK, 2011).

[10]R. Scheer and H. W. Schock, *Chalcogenide Photovoltaics: Physics, Technologies, and Thin Film Devices* (Wiley-VCH, Weinheim, Germany, 2011).

[11]E. H. Putley, *The Hall Effect and Related Phenomena* (Butterworths, London, UK, 1960).

[12]P. Blood and J. W. Orton, *The Electrical Characterization of Semiconductors: Majority Carriers and Electron States* (Academic Press, London, UK, 1992).

[13]A. Beer, "The Hall effect and related phenomena," Solid-State Electron. **9**, 339–351 (1966).

[14]D. C. Look, C. E. Stutz, J. R. Sizelove, and K. R. Evans, "On Hall scattering factors for holes in GaAs," J. Appl. Phys. **80**, 1913–1915 (1996).

[15]V. A. Johnson and K. Lark-Horovitz, "Theoretical Hall coefficient expressions for impurity semiconductors," Phys. Rev. **79**, 176 (1950).

[16]B. Gelmont and M. S. Shur, "Hall factor for ionized impurity scattering," J. Appl. Phys. **78**, 2846 (1995).

[17]ASTM Standard F76-86, "Standard method for measuring hall mobility and hall coefficient in extrinsic semiconductor single crystals," in *1991 Annual Book of ASTM Standards* (American Society for Testing Materials, Philadelphia, USA, 1991).

[18]J. W. Orton and M. J. Powell, "The Hall effect in polycrystalline and powdered semiconductors," Rep. Prog. Phys. **43**, 1263 (1980).

[19]J. Crêpellière, P. L. Popa, N. Bahlawane, R. Leturcq, F. Werner, S. Siebentritt, and D. Lenoble, "Transparent conductive CuCrO$_2$ thin films deposited by pulsed injection metal organic chemical vapor deposition: Up-scalable process technology for an improved transparency/conductivity trade-off," J. Mater. Chem. C **4**, 4278–4287 (2016).

[20]M. S. Bennett, "Relationship between Hall constant and carrier densities in polycrystalline semiconductor film," J. Appl. Phys. **58**, 3470 (1985).

[21]J. Jerhot and V. Snejdar, "Hall effect in polycrystalline semiconductors," Thin Solid Films **52**, 379–395 (1978).

[22]M. V. Garcia-Cuenca, J. L. Morenza, and J. M. Codina, "On the Hall effect in polycrystalline semiconductors," J. Appl. Phys. **58**, 1080 (1985).

[23]Y. M. Gal'perin, E. P. German, and V. G. Karpov, "Hall effect under hopping conduction conditions," Sov. Phys. JETP **72**, 193–200 (1991) [Zh. Eksp. Teor. Fiz. **99**, 343–356 (1991) (in Russian)].

[24]S. Atakulov, "To the problem of Hall "mobility" in polycrystalline thin films with potential barriers," Solid State Commun. **51**, 415–419 (1984).

[25]F. Werner, T. Bertram, J. Mengozzi, and S. Siebentritt, "What is the dopant concentration in polycrystalline thin-film Cu(In,Ga)Se$_2$?," Thin Solid Films **633**, 222–226 (2017).

[26]H. Brooks, "Scattering by ionized impurities in semiconductors," Phys. Rev. **83**, 879 (1951).

[27]N. Sclar, "Neutral impurity scattering in semiconductors," Phys. Rev. **104**, 1559–1561 (1956).

[28]E. Z. Dziuba, "Galvanomagnetic properties of HgTe in strong magnetic fields," Phys. Status Solidi B **62**, 307–312 (1974).

[29]J. S. Kim, D. G. Seiler, and W. F. Tseng, "Multicarrier characterization method for extracting mobilities and carrier densities of semiconductors from variable magnetic field measurements," J. Appl. Phys. **73**, 8324 (1993).

[30]W. A. Beck and J. R. Anderson, "Determination of electrical transport properties using a novel magnetic field-dependent Hall technique," J. Appl. Phys. **62**, 541–554 (1987).

[31]J. Antoszewski, D. J. Seymour, L. Faraone, J. R. Meyer, and C. A. Hoffman, "Magneto-transport characterization using quantitative mobility-spectrum analysis," J. Electron. Mater. **24**, 1255–1262 (1995).

[32]I. Vurgaftman, J. R. Meyer, C. A. Hoffman, D. Redfern, J. Antoszewski, L. Faraone, and J. R. Lindemuth, "Improved quantitative mobility spectrum analysis for Hall characterization," J. Appl. Phys. **84**, 4966–4973 (1998).

[33]S. Kiatgamolchai, M. Myronov, O. A. Mironov, V. G. Kantser, E. H. C. Parker, and T. E. Whall, "Mobility spectrum computational analysis using a maximum entropy approach," Phys. Rev. E **66**, 036705 (2002).

[34]J. Rothman, J. Meilhan, G. Perrais, J.-P. Belle, and O. Gravrand, "Maximum entropy mobility spectrum analysis of HgCdTe heterostructures," J. Electron. Mater. **35**, 1174–1184 (2006).